

Stacked Nonnegative Sparse Autoencoders for Robust Hyperspectral Unmixing

Yuanchao Su¹, *Student Member, IEEE*, Andrea Marinoni², *Senior Member, IEEE*,
Jun Li¹, *Senior Member, IEEE*, Javier Plaza³, *Senior Member, IEEE*,
and Paolo Gamba⁴, *Fellow, IEEE*

Abstract—As an unsupervised learning tool, autoencoder has been widely applied in many fields. In this letter, we propose a new robust unmixing algorithm that is based on stacked nonnegative sparse autoencoders (NNSAEs) for hyperspectral data with outliers and low signal-to-noise ratio. The proposed stacked autoencoders network contains two main steps. In the first step, a series of NNSAE is used to detect the outliers in the data. In the second step, a final autoencoder is performed for unmixing to achieve the endmember signatures and abundance fractions. By taking advantage from nonnegative sparse autoencoding, the proposed approach can well tackle problems with outliers and low noise-signal ratio. The effectiveness of the proposed method is evaluated on both synthetic and real hyperspectral data. In comparison with other unmixing methods, the proposed approach demonstrates competitive performance.

Index Terms—Deep learning, hyperspectral remote sensing, nonnegative sparse autoencoder (NNSAE), unmixing.

I. INTRODUCTION

HYPERSPECTRAL images have been widely used in modern geophysical applications, such as classification, target detection, urban monitoring, and so on. However, due to the relatively low-spatial resolution of hyperspectral images, many pixels would be mixed by several pure spectral materials (endmembers), which brings difficulty for the characterization of hyperspectral data and might lead to dramatic inaccuracy in the understanding and quantifying the considered scenes [1].

In order to deal with mixed pixels, many algorithms have been proposed for hyperspectral unmixing in the literature [1].

Manuscript received November 8, 2017; revised April 4, 2018; accepted May 16, 2018. Date of publication June 18, 2018; date of current version August 27, 2018. This work was supported in part by the National Natural Science Foundation of China under Grant 61771496, in part by the National Key Research and Development Program of China under Grant 2017YFB0502900, and in part by Guangdong Provincial Natural Science Foundation under Grant 2016A030313254. (*Corresponding author: Jun Li.*)

Y. Su and J. Li are with the Guangdong Provincial Key Laboratory of Urbanization and Geo-simulation, Center of Integrated Geographic Information Analysis, School of Geography and Planning, Sun Yat-sen University, Guangzhou 510275, China (e-mail: suyuch3@mail2.sysu.edu.cn; lijun48@mail.sysu.edu.cn).

J. Plaza is with the Hyperspectral Computing Laboratory, Department of Technology of Computers and Communications, Escuela Politécnica, University of Extremadura, E-10071 Cáceres, Spain.

A. Marinoni and P. Gamba are with the Dipartimento di Ingegneria Industriale e dell'Informazione, Università degli Studi di Pavia, I-27100 Pavia, Italy.

Color versions of one or more of the figures in this letter are available online at <http://ieeexplore.ieee.org>.

Digital Object Identifier 10.1109/LGRS.2018.2841400

Based on the fact that whether training samples are involved in the process or not, most methods can be classified into two categories, i.e., hand-crafted and learning based. Hand-crafted methods, such as N-FINDR [2], vertex component analysis (VCA) [3], minimum volume constrained nonnegative matrix factorization (MVC-NMF) [4], focus on exploiting the data structure via some geometrical or statistical assumptions, and exhibiting good performance in unmixing. The hand-crafted methods were the main trend in the past two decades, and shown to be very effective in many scenarios. However, the existence of outliers restricts the full play of these methods [5].

Recently, the fast development of artificial neural networks (ANNs) has fostered the learning-based approaches for unmixing [6]. The ANN-based approaches were first developed for the learning of abundance fractions, implying the knowledge of the endmember signatures [7]. Those approaches showed better performance in comparison with the hand-crafted methods, due to the strong interpretable ability of its deep features [7]. More recently, the nonnegative sparse autoencoder (NNSAE), as a special case of ANN, was employed to obtain the endmembers signatures and abundance fractions simultaneously for unmixing [8], with advanced denoising and intrinsic self-adaptation capabilities. However, as its strength is in the aspect of antinoise, in case of outliers, it results in strong limitations. Because outliers might lead to initialization failure, the presence of outliers can bring strong interference to its unmixing results.

The main contribution of this letter is that, we propose a stacked NNSAEs architecture, namely, stacked NNSAEs (SNSAs), for hyperspectral unmixing, aiming at tackling the outliers and low noise-signal ratio in the data. As a combination of stacked standard autoencoders, the proposed SNSA adopts two additional criteria, with a sparse one enhancing the training efficiency and a nonnegativity constraining the estimated abundance. As illustrated in Fig. 1, the proposed SNSA first has a group of autoencoders, which aims at detecting the outliers. Then, the last autoencoder implements the matrix decomposition with sparse autoencoding targeting on spectral unmixing.

The remainder of this letter is organized as follows. Section II describes the proposed SNSA approach. In Section III, simulated data sets are used for evaluation, which allow us to conduct a quantitative comparison with

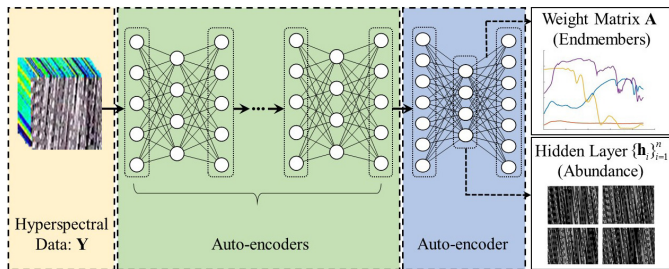


Fig. 1. Flowchart of the proposed SNSA approach. The first group of autoencoders aims at outlier detection. The last autoencoder is employed for unmixing.

other methods. In Section IV, experiments with two real hyperspectral data are conducted for further validation. Section V concludes this letter with some remarks.

II. PROPOSED APPROACH

In this section, we present the proposed SNSA for hyperspectral data unmixing. Following the linear spectral mixing model, this letter assumes that the reflected spectra are linearly mixed by several endmembers. Hence, for a given observation $\mathbf{y}_i \in \mathbb{R}^l$ with l being the number of bands, we have

$$\begin{aligned} \mathbf{y}_i &= \mathbf{A}\mathbf{h}_i + \boldsymbol{\varepsilon}_i = \sum_{j=1}^m h_{ij} \mathbf{a}_j + \boldsymbol{\varepsilon}_i \\ \text{s.t. } \mathbf{h}_i &\geq 0, \quad \sum_{j=1}^m h_{ij} = 1 \end{aligned} \quad (1)$$

where $\mathbf{A} = [\mathbf{a}_1, \dots, \mathbf{a}_m] \in \mathbb{R}^{l \times m}$ is the endmember matrix with m being the number of endmembers, $\mathbf{h}_i = [h_{i1}, \dots, h_{im}]^T \in \mathbb{R}^m$ denotes the abundance fractions with h_{ij} corresponding to the j th endmember, and $\boldsymbol{\varepsilon}_i$ is the error vector. The two constraints $\mathbf{h}_i \geq 0$ and $\sum_{j=1}^m h_{ij} = 1$ are the abundance nonnegativity constraint and abundance sum-to-one constraint, respectively [9].

In the following, we will present the proposed SNSA. Specifically, in Section II-A, we briefly review the NNSAE algorithm and introduce how to detect outliers. Section II-B describes the NNSAE for unmixing.

A. Group of Autoencoders for Outlier Detection

As the optimization problem involved in the network is nonconvex, an even worse scenario is the presence of outliers, which can bring strong interference to the solution.

We first run VCA to obtain k endmembers as candidates with $k > m$, which are then grouped into m training sets $\{\mathbf{S}_j\}_{j=1}^m$ based on spectral angle distances (SADs) with $\mathbf{S}_j = [\mathbf{a}_1, \dots, \mathbf{a}_{j_n}]$ and j_n be the number of samples in \mathbf{S}_j . It is worth noting that besides VCA, any other pure pixel-based methods can be used for initialization of the training, as the outliers are likely to be selected since they are shown to be vertices. Furthermore, for the number of candidates, we set $k = 2m$ and repeated VCA for 30 times in this letter.

Let $\hat{\mathbf{a}}_j$ be the reconstructed signature of the j th candidate, we can obtain

$$\hat{\mathbf{a}}_j = \mathbf{W}_j^{\text{output}} \mathbf{f}(\mathbf{W}_j^{\text{input}} \mathbf{S}_j) \quad (2)$$

where $\mathbf{f}(\cdot)$ is an activation function, $\mathbf{W}_j^{\text{input}} \in \mathbb{R}^{l \times l}$ is a matrix of weights from the input layer to the hidden layer, and $\mathbf{W}_j^{\text{output}} \in \mathbb{R}^{l \times l}$ is a matrix of connection weights between the hidden layer and the output layer. In the group of autoencoders, the number of hidden neurons is set as the number of bands l in the hyperspectral data. In practice, we generally share the weights between the input and hidden neurons with those from hidden to output neurons, which means $\mathbf{W}_j = \mathbf{W}_j^{\text{output}} = (\mathbf{W}_j^{\text{input}})^T$. Therefore, the problem (2) turns to

$$\hat{\mathbf{a}}_j = \mathbf{W}_j \mathbf{f}(\mathbf{W}_j^T \mathbf{S}_j). \quad (3)$$

The learning of the autoencoder aims at minimizing the reconstruction error (RE) as follows:

$$\min \sum_{i=1}^{j_n} \|\mathbf{a}_i - \hat{\mathbf{a}}_j\|_2^2.$$

For the activation function $\mathbf{f}(\cdot)$ in (3), herein we adopt the logistic function as follows:

$$\mathbf{f}(\mathbf{g}_j) = \frac{1}{1 + \exp(-\mathbf{c}_j \cdot \mathbf{g}_j - \mathbf{d}_j)} \quad (4)$$

where $\mathbf{g}_j = \mathbf{W}_j^T \mathbf{S}_j$ and \mathbf{c}_j and \mathbf{d}_j are parameters aiming at controlling the information transmission between neurons.

For the construction of the autoencoders, let $\hat{\mathbf{a}}_j^t$ and $\hat{\mathbf{a}}_j^{t+1}$ be the reconstructions from the t th and $(t+1)$ th autoencoders, respectively. When $\|\hat{\mathbf{a}}_j^{t+1} - \hat{\mathbf{a}}_j^t\|_2^2$ converges, the search of autoencoder ends for the network. Finally, we detect the outliers based on the reconstructed spectral signatures. Let $\gamma_j = [\gamma_{j1}, \dots, \gamma_{jn}]^T$ be the SADs between $\hat{\mathbf{a}}_j^t$ and the samples in \mathbf{S}_j , ν and σ be the mean and standard deviation of γ_j , respectively. Then, we use $\nu + 3\sigma$ as the threshold for the outlier detection. When an outlier \mathbf{y}_o is detected, we set it to the mass center of the estimated endmembers, i.e., $\mathbf{y}_o = (1/m) \sum_{j=1}^m \hat{\mathbf{a}}_j$.

B. Autoencoder for Unmixing

In the second autoencoder, we minimize the RE $(1/n) \sum_{i=1}^n \|\mathbf{y}_i - \mathbf{A}\mathbf{h}_i\|_2^2$, which is the same as the NNSAE learning, in which n is the number of pixel in the considered hyperspectral data set, \mathbf{A} and \mathbf{h}_i are the weight matrix and the neural activity, respectively [10]. Following in the minimum volume assumption that all samples in the data are enclosed by the simplex constructed by the endmembers [4], we employ the MVC into the model as follows:

$$\begin{aligned} \min & \frac{1}{n} \sum_{i=1}^n \|\mathbf{y}_i - \mathbf{A}\mathbf{h}_i\|_2^2 + \mu \text{MinVol}(\mathbf{A}) \\ \text{s.t. } & \mathbf{h}_i \geq 0, \quad \mathbf{1}_m^T \mathbf{h}_i = 1 \end{aligned} \quad (5)$$

where parameter μ is a penalty coefficient, $\text{MinVol}(\mathbf{A})$ is the volume function which is adopted from [4].

Problem (5) is nonconvex and difficult to solve. In the second autoencoder, we adopt NNSAE to learn the weight

Algorithm 1 SNSA for Hyperspectral Unmixing**Require:** $\mathbf{Y} \in \mathbb{R}^{l \times n}$ (data set)**Ensure:** Endmembers $\mathbf{A} \in \mathbb{R}^{l \times m}$, Abundances $\mathbf{H} \in \mathbb{R}^{m \times n}$.**Step 1.** *A group of autoencoders for outlier detection*

1. Run VCA to obtain the training sets $\{\mathbf{S}_j\}_{j=1}^m$
2. Initialize \mathbf{A} via VCA [3]
3. Initialize randomly \mathbf{W}_j

repeat

4. Update $\{\hat{\mathbf{a}}_j\}_{j=1}^m$ in (3)
5. Update $\{\mathbf{W}_j\}_{j=1}^m$ via gradient derivation

until convergence

6. Outlier detection

Step 2. *An autoencoder for unmixing*

7. Initialize \mathbf{A} from VCA
8. \mathbf{h}_i via FCLS [9]
9. Set $\mu = 0.001$, $\eta = 0.01$, $\vartheta = 20$

repeat

10. Update $\Delta \mathbf{A}$ in (6)
11. Update $\Delta \mathbf{h}_i$ in (8)

until convergence

matrix \mathbf{A} and the neural activities, respectively, via an iterative scheme. Specifically, with respect to the weight matrix \mathbf{A} , we have $\mathbf{A} \leftarrow \mathbf{A} + \Delta \mathbf{A}$ with

$$\Delta \mathbf{A} = \eta(\mathbf{y}_i - \mathbf{A}\mathbf{h}_i)\mathbf{h}_i^T + d(\mathbf{A}) + \mu d(\text{MinVol}(\mathbf{A})) \quad (6)$$

where η is the learning rate [10], $d(\mathbf{A})$ and $d(\text{MinVol}(\mathbf{A}))$ are the gradients for the weight matrix and volume function, respectively. The latter one can be computed as that in [4]. For the former one, in order to enforce nonnegativity weights, we employ the asymmetric piecewise linear decay function [10]

$$d(\mathbf{A}) \leftarrow \begin{cases} -a_{ij} & (a_{ij} < 0) \\ 0 & (a_{ij} \geq 0) \end{cases} \quad (7)$$

where a_{ij} is an element in matrix \mathbf{A} , which connects the hidden neuron j and the output neuron i [10]. In this autoencoder, the number of hidden neurons is set as the number of endmembers.

On the other hand, with respect to the neural activity \mathbf{h}_i , we herein employ the gradient descent for the solution $\mathbf{h}_i \leftarrow \mathbf{h}_i + \Delta \mathbf{h}_i$ as follows:

$$\Delta \mathbf{h}_i = \varphi \bar{\mathbf{A}}^T (\bar{\mathbf{A}}\mathbf{h}_i - \bar{\mathbf{y}}_i) \quad (8)$$

where the parameter φ can be estimated by the Armijo rule [11], $\bar{\mathbf{A}}$ and $\bar{\mathbf{y}}_i$ are the augmented matrices, $\bar{\mathbf{A}} = [\mathbf{A}; \vartheta \mathbf{1}_m^T]$ and $\bar{\mathbf{y}}_i = [\mathbf{y}_i; \vartheta \mathbf{1}_n^T]$ with ϑ being a coefficient balance. Following the analysis in [4], we set $\vartheta = 20$ as a hyperparameter. Finally, the pseudocode of the proposed SNSA algorithm is shown in Algorithm 1. Step 1 is the first group of the network, while lines 1–3 perform the initialization and lines 4–5 aim at removing outliers in the data. Then, step 2 is the last autoencoder of the network which conducts spectral unmixing via NMF. Lines 7–9 set the initial conditions. Lines 10 and 11 update the endmember matrix and abundance fractions, respectively. As for the convergence performance,

TABLE I

SAD (IN RADIANS), RMSE, AND RE RESULTS ALONG WITH THEIR STANDARD DEVIATIONS OBTAINED FROM 10 MONTE CARLO RUNS BY USING DIFFERENT PARAMETERS FROM THE PROPOSED SNSA FOR A SCENARIO WITH 4 ENDMEMBERS, 10 OUTLIERS, AND SNR = 30 dB

		SAD	RMSE	RE
$\mu = 0.01$	$\eta = 0.1$	0.0193±2.15%	0.3904±0.25%	0.0146±0.12%
	$\eta = 0.01$	0.0147±1.45%	0.2375±0.20%	0.0121±0.08%
	$\eta = 0.001$	0.0150±1.81%	0.2403±0.22%	0.0129±0.09%
$\mu = 0.001$	$\eta = 0.1$	0.0138±1.57%	0.3204±0.41%	0.0126±0.08%
	$\eta = 0.01$	0.0120±1.19%	0.1931±0.10%	0.0109±0.01%
	$\eta = 0.001$	0.0127±1.32%	0.2035±0.14%	0.0113±0.02%
$\mu = 0.0001$	$\eta = 0.1$	0.0140±1.62%	0.2739±0.32%	0.0151±0.10%
	$\eta = 0.01$	0.0112±1.24%	0.2064±0.15%	0.0149±0.03%
	$\eta = 0.001$	0.0121±1.39%	0.2096±0.25%	0.0157±0.07%

in practice, if $\|\Delta \mathbf{A}\|_F^2$, where $\|\cdot\|_F$ denotes the Frobenius norm, is smaller than a threshold, both autoencoders terminate. It should be noted that the parameters involved in the algorithm are set empirically. We are aware that there are ways to optimize these settings. Nevertheless, we empirically found out that the algorithm is not sensitive to the settings. Furthermore, as can be observed from the experimental results presented in Section III, these settings lead to very good performance.

III. EXPERIMENTAL RESULTS WITH SIMULATED DATA

The effectiveness of the proposed SNSA is evaluated by using simulated hyperspectral data. The simulated data are generated according to a linear mixing model with 3364 pixels with maximum abundance purity of 0.8. Two different scenarios, with 3 and 4 endmembers, are considered, where the pure spectral signatures, with 224 spectral bands covering the spectral range from 0.4 to 2.5 μm , are randomly selected from the United States Geological Survey (USGS) library. Finally, as the main target of the proposed approach is outliers and low SNR, 10 outliers and white Gaussian noise with two different levels of SNR, i.e., 15 and 30 dB, are added in the synthetic data.

Three indicators, i.e., the SAD, RE, and the root-mean-square error (RMSE) are used to measure the accuracy of the unmixing results which are given as follows:

$$\begin{cases} \text{SAD}[\mathbf{a}_j, \hat{\mathbf{a}}_j] = \arccos \left(\frac{[\mathbf{a}_j, \hat{\mathbf{a}}_j]}{\|\mathbf{a}_j\| \cdot \|\hat{\mathbf{a}}_j\|} \right) \\ \text{RE}(\{\mathbf{y}_i\}_{i=1}^n, \{\hat{\mathbf{y}}_i\}_{i=1}^n) = \frac{1}{n} \sum_{i=1}^n \sqrt{\|\mathbf{y}_i - \hat{\mathbf{y}}_i\|_2^2} \\ \text{RMSE}(\hat{\mathbf{h}}_i, \mathbf{h}_i) = \frac{1}{n} \sum_{i=1}^n \sqrt{\|\mathbf{h}_i - \hat{\mathbf{h}}_i\|_2^2} \end{cases}$$

where $\hat{\mathbf{a}}_j$ and \mathbf{a}_j are the extracted endmember signature and the library spectrum, $\hat{\mathbf{y}}_i$ and \mathbf{y}_i are the reconstruction and observation of pixel i , and $\hat{\mathbf{h}}_i$ and \mathbf{h}_i are the corresponding estimated and actual abundance fractions, respectively.

In the first experiment, we perform an analysis on the network parameters, for the considered hyperspectral data with 4 endmembers, 10 outliers, and SNR = 30 dB. Table I gives the obtained results with different parameter settings. It can first be observed that the proposed SNSA is insensitive to the settings. Within a relevant wide range, $\eta \in [0.001, 0.1]$,

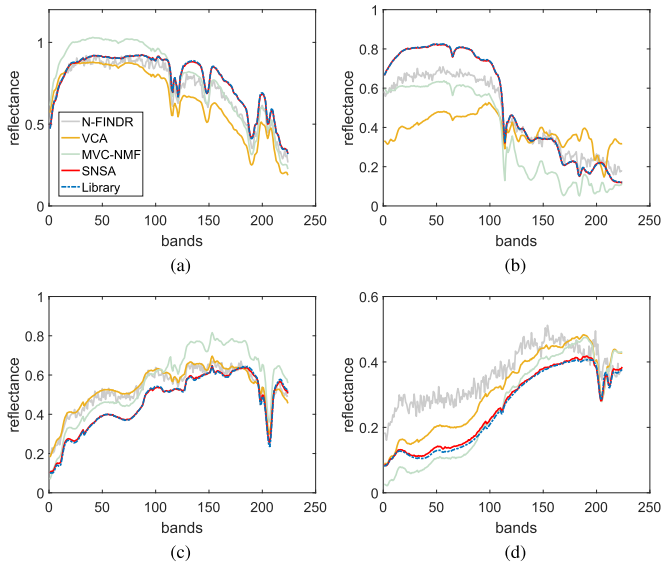


Fig. 2. Comparison between the reference USGS library spectra and the estimated endmembers by the proposed method for the problem with 4 endmembers, 10 outliers, and SNR = 30 dB. (a) Endmember 1. (b) Endmember 2. (c) Endmember 3. (d) Endmember 4.

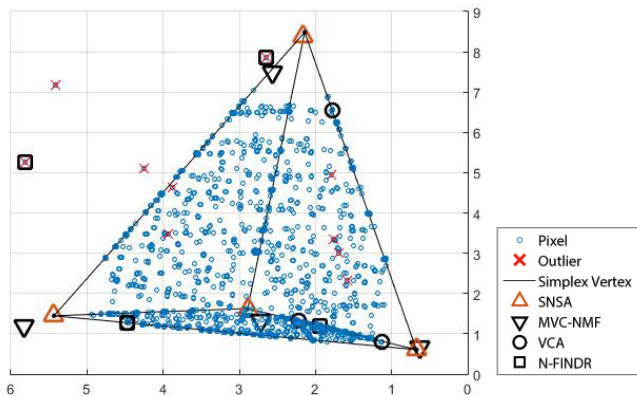


Fig. 3. Scatter plot of the obtained results for the synthetic data with 4 endmembers, 10 outliers, and SNR = 30 dB.

$\mu \in [0.0001, 0.01]$, the proposed SNSA can obtain good results. In the following experiments, we set $\mu = 0.001$ and $\eta = 0.01$ for the proposed algorithm.

Our proposed method is compared with three widely used unmixing algorithms, i.e., N-FINDR [1], VCA [3], and MVC-NMF [4]. First of all, Figs. 2 and 3 show a comparison between the obtained endmembers and the reference USGS library signatures for the problem of 4 endmembers and SNR = 30 dB. It can be seen from these figures that the proposed method provides better match between the library spectra and the endmembers provided than the other methods. In fact, SNSA is able to retrieve more accurate and smooth estimates of the endmember signatures by taking advantage of the outlier detection and the neural network training. Furthermore, for quantitative analysis, Table II presents the obtained SADs, RMSEs, and REs for different SNRs. From the results reported in Table II, it can be observed that the proposed SNSA obtained the best results.

TABLE II
AVERAGE SADs (IN RADIANs), REs, AND RMSEs ALONG WITH THEIR STANDARD DEVIATIONS OBTAINED FROM 10 MONTE CARLO RUNS BY DIFFERENT METHODS FOR THE CONSIDERED SIMULATED DATA. THE BOLD NUMBERS REPRESENT THE BEST RESULTS

Method	SAD	RMSE		RE
		m = 3, SNR = 30 dB		
N-FINDR	0.6017±14.35%	0.3946±3.12%	0.0193±0.84%	
VCA	0.5924±11.02%	0.4721±2.36%	0.0186±0.99%	
MVC-NMF	0.1958±9.36%	0.2513±1.15%	0.0127±0.52%	
SNSA	0.0113±1.13%	0.1984±0.11%	0.0108±0.01%	
m = 4, SNR = 15 dB				
N-FINDR	0.9375±31.85%	0.8264±8.16%	0.0579±4.95%	
VCA	0.8019±23.61%	0.7516±5.34%	0.0653±5.62%	
MVC-NMF	0.3124±15.52%	0.7433±2.27%	0.0524±2.10%	
SNSA	0.0437±5.32%	0.5394±1.19%	0.0413±0.75%	

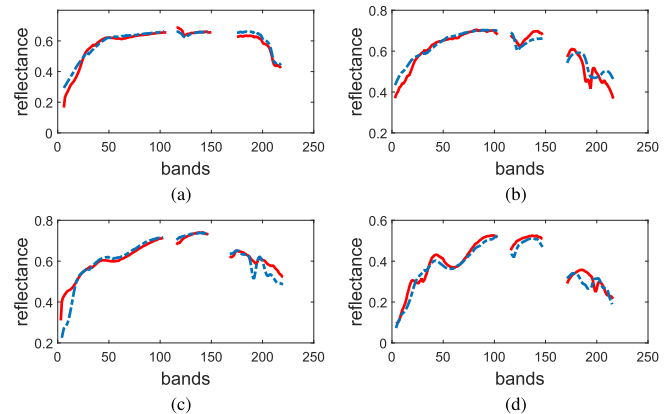


Fig. 4. Experimental results via SNSA on Cuprite data. Comparison of the estimated endmembers (red) with their corresponding library signatures (blue). (a) Buddingtonite. (b) Chalcedony. (c) Montmorillonite. (d) Nontronite.

TABLE III
SADs (IN RADIANs) AND REs ALONG WITH THEIR STANDARD DEVIATIONS OBTAINED FROM 10 MONTE CARLO RUNS OBTAINED BY DIFFERENT METHODS FOR THE CUPRITE DATA, WHERE THE BEST RESULTS ARE IN BOLD

Mineral	N-FINDR	VCA	MVC-NMF	SNSA
Alunite	0.0992±0	0.1027±4.72%	0.1218±2.13%	0.1193±2.94%
Buddingtonite	0.1639±0	0.1495±3.65%	0.1085±5.34%	0.1069±3.52%
Chalcedony	0.1687±0	0.1594±1.47%	0.1038±1.26%	0.1097±4.08%
Jarosite	0.1893±0	0.1567±4.40%	0.1195±3.57%	0.1201±3.62%
Kaolinite # 1	0.0804±0	0.0797±3.94%	0.0842±4.28%	0.0829±5.57%
Kaolinite # 2	0.0883±0	0.0895±1.52%	0.0873±3.19%	0.0859±4.03%
Kaolinite # 3	0.0585±0	0.0592±2.08%	0.0603±3.35%	0.0599±3.27%
Montmorillonite	0.0651±0	0.0589±2.25%	0.0615±4.47%	0.0591±6.01%
Muscovite	0.1437±0	0.1302±1.86%	0.1291±2.05%	0.1242±1.79%
Nontronite	0.0803±0	0.0795±5.13%	0.0824±3.69%	0.0783±2.84%
Pyrope # 1	0.0532±0	0.0519±4.32%	0.0537±5.01%	0.0521±4.76%
Pyrope # 2	0.0701±0	0.0694±2.17%	0.0686±3.78%	0.0680±3.38%
Mean SAD	0.1051	0.0989	0.0901	0.0889
RE	0.0090±0	0.0052±0.07%	0.0039±0.08%	0.0040±0.07%

IV. EXPERIMENTS WITH REAL HYPERSPECTRAL DATA

In this experiments, two real hyperspectral data, the Cuprite image [12], and Jasper Ridge image [13], are considered.

The first real hyperspectral data with 191×250 pixels, collected by the Airborne Visible Infra-Red Imaging Spectrometer (AVIRIS) data over the Cuprite mining site, Nevada, in 1997 [12], are used for further validation of our proposed approach. This scene has 224 spectral bands over a wavelength from 0.4 to 2.5 μm , with a nominal spectral resolution of

TABLE IV
SADS (IN RADIANs) AND RES ALONG WITH THEIR STANDARD DEVIATIONS OBTAINED FROM 10 MONTE CARLO RUNS OBTAINED BY DIFFERENT METHODS FOR THE JASPER RIDGE DATA, WHERE THE BEST RESULTS ARE IN BOLD

Mineral	N-FINDR	VCA	MVC-NMF	SNSA
Road	0.0906 ±0%	0.1004±2.71%	0.0914±3.05%	0.0909±1.82%
Soil	0.2253±0%	0.2150 ±1.59%	0.2208±2.24%	0.2181±1.61%
Tree	0.1559 ±0%	0.1801±4.71%	0.1713±2.53%	0.1679±2.18%
Water	0.1337±0	0.1324±2.46%	0.1282±3.00%	0.1263 ±1.97%
Mean SAD	0.1514	0.1570	0.1529	0.1508
RE	0.0101±0	0.0107±0.10	0.0098±0.09	0.0095 ±0.08

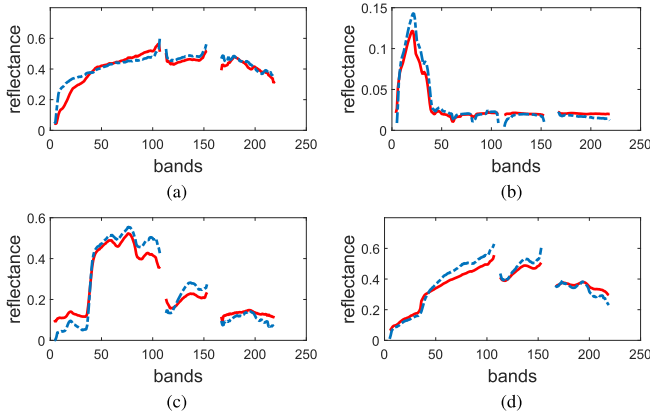


Fig. 5. Experimental results via SNSA on Jasper Ridge data. Comparison of the estimated endmembers (red) with their corresponding reference signatures (blue). (a) Road. (b) Soil. (c) Tree. (d) Water.

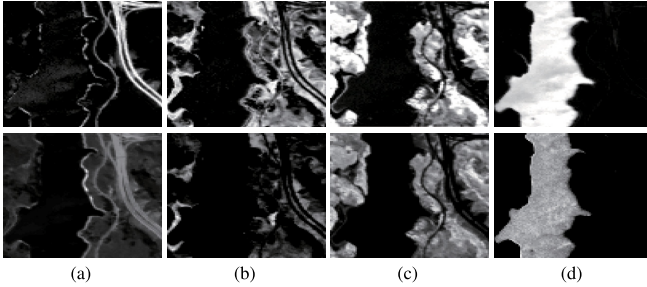


Fig. 6. (Top) Ground-truth abundance maps on Jasper Ridge data. (Bottom) Estimated abundance maps by the proposed SNSA. (a) Road. (b) Soil. (c) Tree. (d) Water.

10 nm. Prior to the analysis, bands 1–2, 105–115, 150–170, and 223–224 were removed due to water absorption and low SNR in those bands, leaving a total of 188 spectral bands.

In this experiment, we set the number of endmembers as $m = 12$. The signatures obtained by the proposed SNSA are presented in Fig. 4, from which it can be observed that the estimated endmember signatures generally provide a good match with regard to the corresponding ones in the library. For further validation, quantitative results are displayed in Table III, which illustrate that the obtained SADs are better or competitive to those of the other algorithms. Specifically, it is possible to appreciate that the proposed approach outperforms the other methods in terms of mean SAD, i.e., SNSA is able to retrieve more stable abundance estimates by means of its accurate endmember detection.

The second real data, with 100×100 pixels, is captured by AVIRIS over Jasper Ridge in California [13]. The scene has 224 bands over a wavelength from 0.38 to 2.5 μm . After the removal of water absorption and low-SNR bands, including 1–3, 108–112, 154–166, and 220–224 bands, 162 spectral bands are used for experiment. The number of endmembers considered in this experiment is set as $m = 4$. The quantitative results are listed in Table IV, from which we can observe that that proposed SNSA obtained competitive or comparable results in comparison with other methods. For illustrative purposes, the abundance map and signatures are shown in Figs. 5 and 6, respectively, which can further demonstrate the effectiveness of the proposed approach.

V. CONCLUSION

In this letter, we have introduced a new approach, namely, SNSA network for hyperspectral unmixing. By taking advantage from outlier detection and neural network training, SNSA is able to retrieve accurate extraction of endmember signatures and precise abundance estimates. The experimental results, obtained by using simulated and real hyperspectral data, indicate that the proposed SNSA exhibits very good potential for unmixing.

REFERENCES

- [1] J. M. Bioucas-Dias *et al.*, “Hyperspectral unmixing overview: Geometrical, statistical, and sparse regression-based approaches,” *IEEE J. Sel. Topics Appl. Earth Observ. Remote Sens.*, vol. 5, no. 2, pp. 354–379, Apr. 2012.
- [2] M. E. Winter, “N-FINDR: An algorithm for fast autonomous spectral endmember determination in hyperspectral data,” in *Proc. SPIE Image Symp. V*, vol. 3753, 1999, pp. 266–277.
- [3] J. M. P. Nascimento and J. M. Bioucas-Dias, “Vertex component analysis: A fast algorithm to unmix hyperspectral data,” *IEEE Trans. Geosci. Remote Sens.*, vol. 43, no. 4, pp. 898–910, Apr. 2005.
- [4] L. Miao and H. Qi, “Endmember extraction from highly mixed data using minimum volume constrained nonnegative matrix factorization,” *IEEE Trans. Geosci. Remote Sens.*, vol. 45, no. 3, pp. 765–777, Mar. 2007.
- [5] M. Toomik, S. Lu, and J. D. B. Nelson, “M-estimation for robust sparse unmixing of hyperspectral images,” *Proc. SPIE Image Signal Process. Remote Sens. XXII*, vol. 10004, p. 100040V, 2016.
- [6] J. Plaza and A. Plaza, “Spectral mixture analysis of hyperspectral scenes using intelligently selected training samples,” *IEEE Geosci. Remote Sens. Lett.*, vol. 7, no. 2, pp. 371–375, Apr. 2010.
- [7] G. A. Licciardi and F. D. Frate, “Pixel unmixing in hyperspectral data by means of neural networks,” *IEEE Trans. Geosci. Remote Sens.*, vol. 49, no. 11, pp. 4163–4172, Nov. 2011.
- [8] R. Guo, W. Wang, and H. Qi, “Hyperspectral image unmixing using autoencoder cascade,” in *Proc. 7th Workshop Hyperspectral Image Signal Process., Evol. Remote Sens. (WHISPERS)*, Jun. 2015, pp. 1–4.
- [9] D. C. Heinz and C.-I. Chang, “Fully constrained least squares linear spectral mixture analysis method for material quantification in hyperspectral imagery,” *IEEE Trans. Geosci. Remote Sens.*, vol. 39, no. 3, pp. 529–545, Mar. 2001.
- [10] A. Lemme, R. F. Reinhart, and J. J. Steil, “Online learning and generalization of parts-based image representations by non-negative sparse autoencoders,” *Neural Netw.*, vol. 33, pp. 194–203, Sep. 2012.
- [11] J. Nocedal and S. J. Wright, *Numerical Optimization*. New York, NY, USA: Springer, 2006, pp. 33–36.
- [12] R. O. Green *et al.*, “Imaging spectroscopy and the Airborne Visible/Infrared Imaging Spectrometer (AVIRIS),” *Remote Sens. Environ.*, vol. 65, no. 3, pp. 227–248, Sep. 1998.
- [13] F. Zhu, Y. Wang, B. Fan, S. Xiang, G. Meng, and C. Pan, “Spectral unmixing via data-guided sparsity,” *IEEE Trans. Image Process.*, vol. 23, no. 12, pp. 5412–5427, Dec. 2014.